M31 Globular Clusters in the HST Archive: I. Cluster Detection and Completeness[1]

Pauline Barmby[2] & John P. Huchra

Harvard-Smithsonian Center for Astrophysics, 60 Garden St., Cambridge, MA 02138

pbarmby@cfa.harvard.edu, huchra@cfa.harvard.edu

ABSTRACT

Globular clusters at the distance of M31 have apparent angular sizes of a few arcseconds. While many M31 GCs have been detected and studied from ground-based images, the high spatial resolution of HST allows much more robust detection and characterization of star cluster properties. We present the results of a search of 157 HST/WFPC2 images of M31, We found 82 previously-cataloged globular cluster candidates as well as 32 new globular cluster candidates and 20 open cluster candidates. We present images of the new candidates and photometry for all clusters. We assess existing cluster catalogs' completeness and use the results to estimate the total number of GCs in M31 as 460 ± 70. The specific frequency is $S_N = 1.2 \pm 0.2$ and the mass specific frequency $T = 2.4 \pm 0.4$; these values are at the upper end of the range seen for spiral galaxies.

Subject headings: galaxies: individual (M31) – galaxies: star clusters – globular clusters: general

1. Introduction

Globular clusters (GCs) are among the oldest surviving stellar objects in the universe. They provide collections of Population II stars with homogeneous abundances and histories, and unique stellar dynamical conditions. The Milky Way's globular cluster system (GCS) is the prototypical one, and its study has contributed much to our knowledge of stellar evolution and galactic structure. It is important to make sure that conclusions drawn from this study are not biased either because the Milky Way's GCS is somehow unusual or because our location in the Galaxy prevents us

[2]Guest User, Canadian Astronomy Data Centre, which is operated by the Herzberg Institute of Astrophysics, National Research Council of Canada.

[1]Based on observations made with the NASA/ESA Hubble Space Telescope, obtained from the data archive at Space Telescope Science Institute. STScI is operated by the Association of Universities for Research in Astronomy, Inc. under NASA contract NAS 5-26555.

from fully characterizing its properties. Globular clusters in Local Group galaxies are particularly valuable for comparison with Milky Way globular clusters. M31 has the Local Group's largest globular cluster population, so it is a natural starting place for studies of extragalactic globular clusters.

The first M31 globular cluster catalog was published by Hubble (1932), followed by Seyfert & Nassau (1945), Vetešnik (1962), Sargent et al. (1977), and Crampton et al. (1985). The most comprehensive recent catalog is that of Battistini et al. (1987); recent works by Battistini et al. (1993) and Mochejska et al. (1998) cover only portions of M31. All of these catalogs contain objects which are not M31 globular clusters: for example, Table 2 of Barmby et al. (2000) lists 199 cluster candidates later shown to be non-clusters. The existing catalogs are also likely to be missing clusters due to magnitude, spatial coverage, and/or resolution limits. Battistini et al. (1993) defined several samples of M31 globular clusters, including a 'confirmed' sample (199 objects), an 'adopted best' sample (298 objects), and an 'extended' sample (356 objects). In Barmby et al. (2000) we compiled a list of clusters and plausible candidates containing 435 objects.

Quantifying the extent of incompleteness and contamination in M31 globular cluster catalogs is extremely important for the interpretation of globular cluster system properties. For example, the spatial distribution of known clusters is flatter, and their globular cluster luminosity function (GCLF) brighter, near the nucleus (Battistini et al. 1993; Barmby et al. 2001a) — is this because the clusters there are truly fewer and brighter, or because existing surveys have not detected the entire cluster population? Even the census of Milky Way clusters is likely to be incomplete: Minniti (1995) estimates that 10–30 Milky Way globulars may be hidden behind the Galactic bulge and therefore missing from current catalogs, which list about 150 objects (Harris 1996). Two such clusters were found by Hurt et al. (2000). It is not unreasonable to suspect that the M31 cluster catalogs could be incomplete by at least a similar fraction.

Ground-based high-resolution imaging and spectroscopy have been used to distinguish M31 globular clusters from interlopers such as foreground stars, background galaxies, and other objects belonging to M31 (e.g., H II regions and open clusters). The bright ($V \lesssim 17$) portion of M31 globular cluster catalogs has been fairly thoroughly examined using one or both of these methods. Racine (1991) and Racine & Harris (1992) used short-exposure CCD images taken in excellent seeing to determine if cluster candidates in the M31 halo were resolved into stars; they found that majority of the halo cluster candidates were background galaxies, not clusters. Radial velocities from optical spectroscopy have also been used by several groups (e.g., Huchra et al. 1982; Federici et al. 1990; Huchra et al. 1991; Federici et al. 1993; Barmby et al. 2000) to eliminate background galaxies and foreground stars from cluster candidate lists. Neither method is infallible, however: compact clusters may be mistaken for background galaxies if not resolved into stars, or for stars if they have a small radial velocity.[3] HST imaging, with its superior spatial resolution, is a useful

[3]Recall that M31 has a heliocentric radial velocity $v_r \approx -300$ km s^{-1}. The velocity range of M31 globular clusters is about +70 to −700 km s^{-1}, and the Galactic models of Ratnatunga, Casertano, & Bahcall (1989) predict that the

tool for removing some of the ambiguities inherent in the ground-based studies.

At the distance modulus of M31 given by Stanek & Garnavich (1998) and Holland (1998) ($(m-M)_0 = 24.47$, $d = 783$ kpc), the angular resolution of HST's WFPC2 camera is equivalent to a spatial resolution of 0.38 pc. is very helpful for the identification of globular clusters in M31. The differences between globular clusters and contaminating objects are much more obvious than with ground-based imaging. M31 has been a popular target for HST: as of 1 December 2000, the Hubble Data Archive contained almost 1100 WFPC2 images within $150'$ of the center of the galaxy. As of the same date, about two dozen M31 globular clusters had been specifically targeted for observation with HST, and the images of these clusters comprise about 20% of all the M31 images. The goal of most targeted HST observations of M31 globular clusters has been the production of color-magnitude diagrams for the clusters and surrounding stellar populations. HST programs which specifically targeted M31 globular clusters include GOs 5112, 5420, 5464, 5907, 6477, 6671, 7826, 8296, and 8664. Our study uses the publicly-available archival data from these programs and many others.

In mid-2000, we began a project to search for globular clusters in archival HST images for the purpose of quantifying the incompleteness of existing cluster catalogs; preliminary results were described in Barmby et al. (2001a). The present paper report the results of our efforts to find globular and other star clusters in archival HST/WFPC2 images and their implications for catalog completeness and contamination. A companion paper (Barmby & Holland 2001) presents measurements of the structural parameters of the clusters and their implications. We do not attempt to construct CMDs for the clusters, since this work is already being carried out by other groups.

2. Searching the HST archive

We searched the HST Archive for all WPFC2 observations with the following properties:

- center of field within $< 150'$ of the center of M31
- broadband filter with central wavelength 300 nm or longer
- total exposure time longer than 100 s.

These parameters were chosen to ensure that we would have a reasonable chance of detecting globular clusters if they were in the image fields. Many images met the requirements, but since most positions had more than one observation per filter and observations in more than one filter, the images comprised only 157 separate fields. Some of these fields were known to contain M31

radial velocities of Milky Way stars with similar colors and magnitudes to M31 globulars are in the range -400 to $+100$ km s^{-1}.

globular clusters; we retained these fields in our search as a check on our ability to identify clusters. We searched the images in only one filter per field. If more than one filter was available, we chose filters in the following order: F555W, F814W, F606W, F450W, F439W, F336W, F300W. (This ordering reflects the distribution filters used for the images combined with our desire to examine as many fields as possible in the same filter.) Information on the fields searched, including dataset name, location, filter, and exposure time is given in Table 1. The images searched are mostly in F555W and F814W, although there is at least one image in each of the filters listed above. The exposure times ranged from 100 to 8400 s. Figure 1 shows the location of all fields on the sky.

We retrieved the images from either the Space Telescope Science Institute or the Canadian Astronomy Data Centre. In both cases the images were pipeline-processed from the raw data at the time of retrieval with the best available calibration images. From STScI we retrieved individual HST images; when multiple images existed for a single field (e.g., in the case of 'cosmic ray-split' images), we combined the images using the IRAF task CRREJ. From CADC we retrieved 'WFPC2 associations'; these are coadded images produced by the CADC pipeline, which combines multiple CR-split images with the GCOMBINE task. We found that GCOMBINE did not adequately remove cosmic-ray hits when only two images were co-added, so in that case we retrieved the individual images and combined them with CRREJ. There were no obvious differences in the images produced using the two methods — we used both since we became aware of availability of association images from the CADC part way into the project.

Once the images were processed, we began the search for star clusters. The first step was carried out 'blind', that is, without any knowledge of the positions of cataloged clusters. Working independently, each of us visually examined each image. PB used SExtractor (Bertin & Arnouts 1996) to automatically identify objects with large areas and/or extended profiles, then visually checked the SExtractor candidates (many of these were actually bright stars) and searched for additional candidates. JH used only visual examination of the images. Bright M31 globular clusters can be visually distinguished from stars and elliptical galaxies because they appear more 'ragged' at the edges (being resolved into stars) and do not have the diffraction spikes seen around bright stars. Faint or small clusters are distinguished more by their image shapes — larger than the point spread function, and less smooth than a galaxy — than by resolution into stars. Clusters are distinguished from H II regions or nebulae by the fact that the latter are much more diffuse are show few individual stars. The visual classification is not completely objective, but it was the best method we could contrive for dealing with the large number of images to be examined and the large number of potential contaminating objects.

Our confidence in the visual classification was bolstered by the fact that we only disagreed on the classification of about 10% of the objects. We re-examined these together to make a final classification. We combined our two lists of cluster candidates to make a final list. Although we were interested primarily in globular clusters, we recorded positions of possible open clusters as well. Following previous authors (e.g., Battistini et al. 1987; Mochejska et al. 1998), we classified our globulars in classes A through D, where A is 'very likely to be a globular cluster' and D is 'likely

not a globular cluster'. We refer to objects in classes A and B as good candidates, and objects in classes C and D as marginal cluster candidates. After generating our final list of cluster candidates, we checked the image positions against existing catalogs of M31 globular clusters. This allowed us to gauge our detection efficiency and locate objects we would otherwise have missed. The globular cluster list used was a 'master list' of globular clusters and candidates, produced by combining the lists of Sargent et al. (1977), Crampton et al. (1985), Battistini et al. (1987), Battistini et al. (1993), and Mochejska et al. (1998); it includes all the objects listed in the Barmby et al. (2000) catalog, plus additional low-probability candidates and non-clusters.

3. Search results

3.1. Globular clusters

We consider the low and high-probability globular clusters separately. 'High probability' are clusters A or B class clusters from Battistini et al. (1987), Battistini et al. (1993), or Mochejska et al. (1998); all other objects are 'low probability'. Racine (1991) showed that the Battistini et al. (1987) classification correlates well with the probability that a candidate will be subsequently shown to be a cluster. 75 high-probability clusters from our master list were located in the HST fields; we detected 71, and some images of previously-cataloged clusters are shown in Figure 2. Three of the four non-detections (138–000, 166–000, and 133–191) appeared to be stars or blends of stars rather than globular clusters; the fourth object was DAO040 and we did not detect any object at the coordinates given by Crampton et al. (1985). Of the 72 low-probability (class C or D) cluster candidates in our HST fields, we found 7 good candidates (000–D038, 000–M91, 020D–089, 097D–000, 132-000, 264–NB19, and NB39), 4 marginal candidates (000–M045, 257–000, NB41 and NB86), and 45 objects which did not appear to be clusters. We did not detect the other 14 objects in our visual search. On re-examining the positions of these objects, we found that none were good or even marginal cluster candidates. Several were clearly stars, and the others were blends of stars or blank fields. Table 2 gives a list of the non-clusters and their classifications.

3.2. Uncataloged globular clusters

Our visual search of the HST fields produced 32 objects not included in any cluster catalog. 10 of these were good candidates, although only about half are as obviously clusters as most of the brighter objects. The good candidates' images are shown in Figure 3. The nature of the remaining 22 objects is unclear. They are clearly not stars; all are at least marginally resolved (FWHM $\gtrsim 0.2''$). However, most are quite faint, and they are not obviously resolved into stars as is the case for most of the globular clusters. They may be blended stars in M31, compact background galaxies, or compact star clusters. We show images of these low-quality objects in Figure 4. Table 3 gives the location and quality of all the new cluster candidates.

3.3. Open clusters

The dividing line between open and globular clusters is somewhat blurred, even in the Milky Way. In their compilation of data on Milky Way globular clusters, Djorgovski & Meylan (1993) note that there are several globulars (BH 176, UKS 2) which could instead be open clusters. In our search, we noted several concentrated objects which could be M31 open clusters. Their nature is uncertain: they could also be low-concentration globulars, or just chance superpositions of stars. Their images are shown in Figure 5. We checked the cluster coordinates against those given in Hodge's (1979) list of M31 open clusters. The coordinates in that catalog have rather low precision ($20''$ in both right ascension and declination), so we searched for coordinate matches within an error circle of radius $30''$. We found 5 matches and attempted to confirm these by comparing the finding charts in Hodge (1982) to our images. The results were inconclusive: either the objects were not clearly identified on the charts, or they were located too close to the edge of the HST image to make a positive identification. We note the possible matches in Table 3.

To see if any of our newly-proposed globular and open cluster candidates had been previously cataloged as background galaxies, we checked their positions against those of galaxies listed in NED.[4] None of the new clusters matched the position of any galaxy listed in NED, although one is listed as a possible H II region (Strauss et al. 1992) and two others may contain radio and X–ray sources (Zhang et al. 1993; Supper et al. 1997). The matches are also noted in Table 3. However, the matches are uncertain since positional uncertainties for the other surveys are large. Figure 6 shows the positions on the sky of all the M31 clusters, both previously-known and newly-discovered. The 'open cluster' near NGC 205 is well outside the disk and is probably not a real cluster.

4. Integrated photometry

After the M31 clusters had been identified on the 'search' images, we retrieved images of their fields in other available filters to extract the most photometric information from the HST Archive. All but 18 clusters had been imaged by WFPC2 in more than one filter. We combined images for cosmic-ray rejection in the same manner used for the search images. Additional processing steps included removing cosmic rays interactively using the IRAF task IMEDIT (this was especially important for non-cosmic-ray-split images) and correcting for warm pixels using the IRAF task COSMICRAYS. While the STSDAS task WARMPIX is the preferred method of dealing with warm pixels, it is slow and requires correction of individual images before they are combined for cosmic ray rejection. Since we had hundreds of individual images to deal with, we chose the more expedient method of treating the warm pixels as if they were as cosmic ray hits on ground-based images. Nearby bright stars and CCD flaws were masked out of the images to prevent contamination of the

[4]The NASA/IPAC Extragalactic Database (NED) is operated by the Jet Propulsion Laboratory, California Institute of Technology, under contract with the National Aeronautics and Space Administration

photometry. A few images were not useful for photometry at all: the globular clusters were either very faint (mostly in the F300W and F336W filters), too close to an image edge, or saturated.

Photometry of extragalactic globular clusters is unfortunately not as simple as photometry of isolated stars or galaxies. There are two key steps in integrated photometry of M31 clusters: measuring the background light, and identifying an appropriate aperture size. The background light consists of two components: unresolved light from the sky and M31, and light from resolved stars in M31 (the latter are a lesser problem in ground-based photometry of M31 GCs since many fewer M31 stars are resolved). Standard background estimators are usually designed to determine the sky background level by rejecting the stars in the background annulus. Since we expect there to be stars overlapping our clusters as well, we estimated the background value for each image as the mean (rather than the more commonly used median or mode) of the pixel values around the image edge, and subtracted it from the image before doing photometry.

Determining the 'correct' aperture size to be used for integrated photometry is non-trivial since the clusters are not all the same size. We estimated the total flux for each object by measuring aperture magnitudes in concentric apertures spaced $0.15''$ apart, plotting magnitude growth curves, and noting where the flux stopped increasing. Using these measurements of the total flux of each cluster, we determined the half-light radius[5] by interpolating the aperture magnitude curves. We calibrated the instrumental magnitudes from the WFPC2 system to the standard system by iteratively solving the equations given in Holtzman et al. (1995), using the charge-transfer-efficiency corrections given by Dolphin (2000). The iterative solution of the calibration equations requires instrumental magnitudes in at least two filters; for objects with only one instrumental magnitude, we fixed the 'standard color' as either the measured ground-based color from Barmby et al. (2000), or if that was unavailable, the average M31 GC color. The results for integrated magnitudes and half-light radii are given in Table 4. In Figure 7, we compare the new HST photometry to the ground-based measurements compiled in Barmby et al. (2000). The agreement is gratifying: the median offset in V is 0.01 ± 0.04 magnitudes, and in I is 0.06 ± 0.04 mag. Most of the large offsets are for objects near the edge of a WFPC2 chip, or whose previous photometry was estimated from photographic plates.

5. Completeness of globular cluster catalogs in M31

To estimate the completeness of globular cluster catalogs in M31, we first need to understand our own detection efficiency. We estimated this by inserting artificial globular clusters into the inner images, for which the distance from the center of M31 $\equiv R_{gc}$ was less than $30'$. The artificial clusters were actually images of the brightest real globular clusters we detected. To insert the

[5]The half-light radius r_h is that which contains half of the integrated cluster light. It should not be confused with the radius at which the surface brightness drops to half of its central value, called variously the core radius r_c, the half-intensity radius, or the half-width at half maximum (HWHM).

artificial clusters, we scaled the image fluxes 0–4 magnitudes fainter, adjusted for the exposure time of the inserted image, rotated the cluster to a random position angle, and applied a random axial ratio from 0.85 to 1.0. This may not have been an entirely correct method of generating artificial clusters, since cluster size, surface brightness, and integrated magnitude are known to be correlated for Milky Way clusters. However, we decided it was better not to introduce additional assumptions about the correlation of these parameters into our detection test. Once an artificial cluster was inserted into a copy of each HST frame, we extracted a $15'' \times 15''$ region around the inserted cluster, and examined only that portion of the image. This cut-out procedure was similar to the procedure used for the re-examination of 'problem' images. In fact the visual examination of the two groups of images was done at the same time, with no reference to which were the inserted clusters and which were the real objects. For each cut-out image, we decided whether or not it was a *bona fide* globular cluster.

The results of our search for the inserted globular clusters are in Figure 8, where detection of each inserted cluster is indicated as a function of V magnitude and R_{gc}. The figure shows, as expected, that our detection efficiency was generally worse for fainter objects and objects near the center of M31. Faint clusters are more difficult to find against the bright background of the M31 disk and nucleus. We also failed to detect a few bright objects, mostly in short exposures or in the near-UV filters F300W and F336W. Overall, we correctly identified 80% of the inserted clusters, and 92% of the objects which appeared in long F555W and F814W exposures.

The distribution of the real globular clusters and candidates detected in the HST images is shown in Figure 9. The number of newly-detected objects increases at fainter magnitudes; there is no clear trend in the number of new objects with R_{gc}. We use the data in Figures 8 and 9 to estimate the completeness of existing catalogs. While it would be desirable to estimate the completeness as a joint function of magnitude and position, the small number of objects we have to work with makes deriving $C(V, R_{gc})$ difficult. Instead we summed over one variable to produce separate functions $C(V)$ and $C(R_{gc})$, which are plotted in Figure 10. The catalog completeness is computed by dividing the number of cataloged objects in a given bin by the true number of objects:

$$C = \frac{N_{\rm cat}}{N_{\rm true}} = \frac{N_{\rm cat}}{N_{\rm cat} + N_{\rm new}/\eta} \tag{1}$$

where the 'true' object total is the sum of the number of cataloged objects and the number of new objects divided by our detection efficiency η. The number of new objects includes the marginal objects. From the results of Racine (1991), only a fraction ($f \lesssim 0.5$) of the marginal objects are likely to be true globular clusters. We therefore give a range of solutions for the completeness functions in Figure 10, corresponding to $f = 0, 0.5$ and 1.0. The figure shows, as expected, that existing catalogs are reasonably complete to $V = 18$, after which the completeness drops drastically. To compute the completeness as a function of R_{gc}, we assumed that detection efficiency at $R_{gc} > 30'$ was the same as that in the $R_{gc} = 30'$ bin. The completeness as a functions of R_{gc} does not follow any particular pattern; the most important point is the low completeness in the innermost bin. $C(R_{gc})$ can only be measured out to about $R_{gc} \leq 70'$, and averaging over this region yields values

for the overall completeness of 50–85%. The small number of objects per radial bin and the uncertainty about the nature of the marginal objects make this estimate rather imprecise.

It is important to know the total number of globular clusters in M31, since it is one of the few spiral galaxies with well-studied GCSs. Existing surveys (summarized in Barmby et al. 2000) and our new HST survey bring the number of confirmed M31 GCs to over 250. The most comprehensive attempt to estimate the total number of M31 GCs (Battistini et al. 1993) gives population ratios $N_{\rm M31}/N_{\rm MW} = 2.5 - 3.5$; with $N_{\rm MW} = 150$, this gives $N_{\rm M31} = 375 - 525$, or 450 ± 75. We can use the results of our completeness study to attempt a new estimate of the total number of M31 GCs. We take two approaches, which use the completeness data somewhat differently. One approach is to use the result that for $V < 18$ and $R_{gc} > 5'$, the existing sample is close to complete. We can therefore use the results of GCLF fitting in this region to estimate the number of clusters fainter than $V = 18$. The GCLFs computed in Barmby et al. (2001a) give a total number of clusters N_{gc} in the range 394–417; the midpoint of the range is 406. In the region $R \leq 5'$, there are 37 cataloged clusters or candidates and the catalog completeness is about 70%. This implies that the true number of clusters is about 53, so the total number of GCs in M31 is approximately $406 + 53 = 459$. A reasonable estimate of the error in this value is 15%, or ± 69.

We can also use the completeness estimates directly, to estimate

$$N_{\rm gc} = \sum_{R_{gc}} \frac{N_{\rm good} + f N_{\rm marg}}{C(R_{gc})} \tag{2}$$

where $N_{\rm good}$ and $N_{\rm marg}$ are the number of good and marginal cataloged clusters in a given R_{gc} bin. The C used in the computation is the value plotted in Figure 10 for the appropriate value of f. The catalog used is that given by Barmby et al. (2000) with likely NGC 205 clusters and (likely young) blue clusters removed. The 299 good clusters are those confirmed by spectroscopy or high-resolution imaging and/or members of the 'adopted best sample' of Battistini et al. (1993); the other 130 clusters are considered marginal. The resulting N_{gc} is sensitive to the value of f and ranges from 415 ± 57 for $f = 0$ to 856 ± 126 for $f = 1.0$. A value of $f = 0.25$, which we believe is reasonable, gives $N_{gc} = 494 \pm 45$. Our two estimates of the total number of GCs in M31 are compatible both with each other and with the results of Battistini et al. (1993). The precision of our results is not much better than that of previous estimates, and improvement will require a wide-field, deep CCD survey of M31 which can be used to find GCs in a uniform manner across the galaxy; such a survey is currently being carried out (Lee et al. 2001).

We now consider implications of our estimated value of M31's N_{gc} for its specific frequency S_N and 'mass specific frequency' T (Zepf & Ashman 1993). To do this we need values for M31's luminosity and mass-to-light ratio. Kent (1987) gives the total magnitude of M31 as $V = 3.28$. Correcting for foreground extinction $A_V = 0.25$ (see Barmby et al. 2000) and our adopted value of $(m - M)_0 = 24.47$ gives $M_V = -21.43$, which is bracketed by the values given by van den Bergh (2001), $M_V = -21.2$, and Ashman & Zepf (1998), $M_V = -21.8$. For ease of comparison we use $M/L_V = 6.1$ as do Kissler-Patig et al. (1999). With $N_{gc} = 459 \pm 69$, this gives $S_N = 1.2 \pm 0.2$

and $T = 2.4 \pm 0.4$. Kissler-Patig et al. (1999) give S_N and T values for seven Sb-Sc spirals in addition to M31. The mean and dispersion of S_N and T for these galaxies are $\langle S_N \rangle = 0.8 \pm 0.2$ and $\langle T \rangle = 1.5 \pm 0.3$. For four Sa and Sab spirals the (highly uncertain) mean values are $\langle S_N \rangle = 2.0 \pm 0.6$ and $\langle T \rangle = 4.0 \pm 1.1$. M31's values of S_N and T fall at the large end of the range of observed values for Sb and Sc spirals, and well within the range observed for Sa and Sab spirals. While it has about twice as many clusters per unit mass or luminosity than the Milky Way, M31 is within the range of variation seen in other spirals' GCSs. It is interesting to speculate on the difference between the Milky Way in M31 in terms of differences in the two galaxies' histories, since obviously environmental differences cannot be a major player. Freeman (1999) suggested that perhaps M31 suffered an early major merger; perhaps this was responsible for the creation of extra GCs in M31, as in the picture of Ashman & Zepf (1992). This would be consistent with the suggestion that some of the metal-rich GCs in M31 are younger than the rest of the population (Barmby & Huchra 2000; Barmby et al. 2001a), although there are not enough metal-rich clusters to account for the entire 'cluster excess' in M31. Further explanation of the total number of clusters in M31 awaits both a larger spiral comparison sample and more detailed theoretical picture of GCS formation.

6. Summary

Using the Hubble Space Telescope Archive to search for M31 globular clusters in WFPC2 images, we present the discovery of many previously-known clusters, a number of new cluster candidates, and some 20 objects which may be M31 open clusters. We use the discovery data, together with an estimate of our discovery efficiency, to estimate the completeness of existing cluster catalogs. As expected, the existing catalogs are least complete for faint clusters and clusters very near the center of M31. As we found in a preliminary version of this analysis in Barmby et al. (2001a), the completeness is very high to the magnitude limit we used for computing the globular cluster luminosity function. This validates our finding that the M31 GCLF varies with both radial distance from the center of M31 and with metallicity.

We use the completeness results to estimate the total number of globular clusters in M31 and derive values in the range 450–500, consistent with or somewhat higher than previous estimates. The specific frequency of GCs in M31 is $S_N = 1.2 \pm 0.2$ and the mass specific frequency $T = 2.4 \pm 0.4$. M31 has more clusters per unit mass or luminosity than the Milky Way, but is within the range of specific frequencies seen in the limited number of other spirals studied to date.

We thank R. Di Stefano, J. Grindlay, D. Sasselov and S. Zepf for helpful discussions.

REFERENCES

Ashman, K. A. & Zepf, S. E. 1992, ApJ, 384, 50

Ashman, K. A. & Zepf, S. E. 1998, Globular Cluster Systems (Cambridge: Cambridge University Press)

Barmby, P. & Huchra, J. P. 2000, ApJ, 531, L29

Barmby, P., Huchra, J. P., & Brodie, J. P. 2001a, AJ, 121, 1482

Barmby, P., Huchra, J. P., Brodie, J. P., Forbes, D. A., Schroder, L. L., & Grillmair, C. J. 2000, AJ, 119, 727

Barmby, P. & Holland, S. 2001, AJ, submitted

Battistini, P. L., Bònoli, F., Braccesi, A., Federici, L., Fusi Pecci, F., Marano, B., & Börngren, F. 1987, A&AS, 67, 447

Battistini, P. L., Bònoli, F., Casavecchi, M., Ciotti, L., Federici, L., & Fusi Pecci, F. 1993, A&A, 272, 77

Bertin, E. & Arnouts, S. 1996, A&AS, 117, 393

Crampton, D., Cowley, A. P., Schade, D., & Chayer, P. 1985, ApJ, 288, 494

Djorgovski, S. & Meylan, G. 1993, in ASP Conf. Proc. 50, Structure and Dynamics of Globular Clusters, ed. S. G. Djorgovski & G. Meylan (San Francisco: ASP), 325

Dolphin, A. E. 2000, PASP, 112, 1397

Federici, L., Bònoli, F., Fusi Pecci, F., Marano, B., Lipovetski, V. A., Niezvestny, S. I., & Spassova, N. 1993, A&A, 274, 87

Federici, L., Marano, B., & Fusi Pecci, F. 1990, A&A, 236, 99

Freeman, K. 1999, in The Stellar Content of Local Group Galaxies, IAU Symposium 192, ed. P. Whitelock & R. Cannon (San Francisco: ASP), 383

Harris, W. H. 1996, AJ, 112, 1487

Hodge, P. W. 1979, AJ, 84, 744

Hodge, P. W. Atlas of the Andromeda Galaxy (Seattle: University of Washington Press)

Holland, S. 1998, AJ, 115, 1916

Holtzman, J. A., Burrows, C. J., Casertano, S., Hester, J. J., Trauger, J. T., Watson, A. M., & Worthey, G. 1995, PASP, 107, 1065

Hubble, E. P. 1932, ApJ, 76, 44

Huchra, J., Stauffer, J., & van Speybroeck, L. 1982, ApJ, 259, L57

Huchra, J. P., Brodie, J. P., & Kent, S. M. 1991, ApJ, 370, 495

Hurt, R. L., Jarrett, T. H., Kirkpatrick, J. D., Cutri, R. M., Schneider, S. E., Skrutskie, M., & van Driel, W. 2000, AJ, 120, 1876

Kent, S. M. 1987, AJ, 94, 306

Kissler-Patig, M., Ashman, K. M., Zepf, S. E., & Freeman, K. C. 1999, AJ, 119, 197

Lee, M. G., Kim, S. C., Geisler, D., Seguel, J., Sarajedini, A., & Harris, W. E. 2001, in Extragalactic Star Clusters, IAU Symposium 207, ed. E. K. Grebel, D. Geisler, & D. Minniti (San Francisco: ASP), 0

Minniti, D. 1995, AJ, 109, 1663

Mochejska, B. J., Kaluzny, J., Krockenberger, M., Sasselov, D. D., & Stanek, K. Z. 1998, Acta Astronomica, 48, 455

Racine, R. 1991, AJ, 101, 865

Racine, R. & Harris, W. E. 1992, AJ, 104, 1068

Ratnatunga, K., Casertano, S., & Bahcall, J. N. 1989, ApJ, 357, 435

Sargent, W. L. W., Kowal, C. T., Hartwick, F. D. A., & van den Bergh, S. 1977, AJ, 82, 947

Seyfert, C. K. & Nassau, J. J. 1945, ApJ, 102, 377

Stanek, K. Z. & Garnavich, P. M. 1998, ApJ, 503, L131

Strauss, M. A., Huchra, J. P., Davis, M., Yahil, A., Fisher, K., & Tonry, J. 1992, ApJS, 83, 29

Supper, R., Hasinger, G., Pietsch, W., Trümper, J., Jain, A., Magnier, E. A., Lewin, W. H. G., & van Paradijs, J. 1997, A&A, 317, 328

van den Bergh, S. 2001, The Galaxies of the Local Group (Cambridge: Cambridge University Press)

Vetešnik, M. 1962, Bull. Astron. Inst. Czech., 13, 180

Zepf, S. E. & Ashman, K. A. 1993, MNRAS, 264, 611

Zhang, X., Zhen, Y., Chen, H., & Wang, S. 1993, A&AS, 99, 545

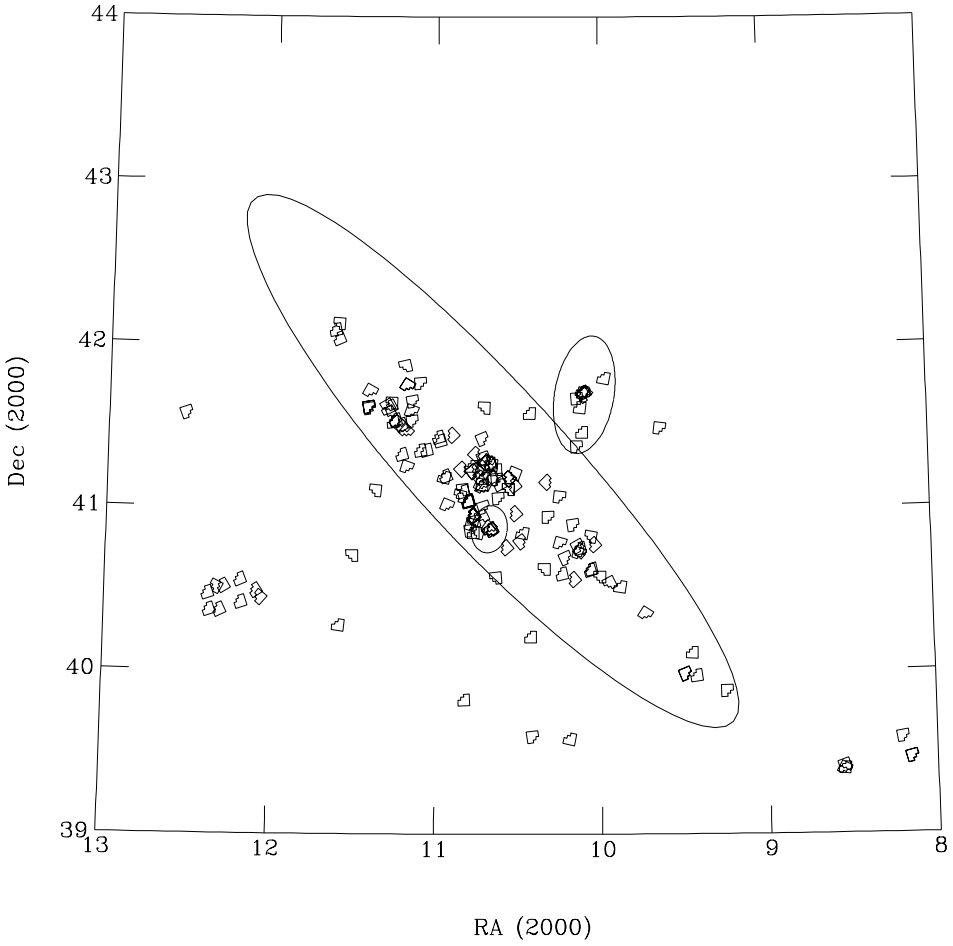

Fig. 1.— Location and orientation of M31 HST fields. Large ellipse is M31 disk/halo boundary as defined by Racine (1991); smaller ellipses are D_{25} isophotes of NGC 205 (NW) and M32 (SE). The WFPC2 symbols are drawn about 1.5× actual size to make them easier to see. The group of fields at $\alpha \sim 12^{\circ}$, $\delta \sim 40.5^{\circ}$ is part of a snapshot survey of field galaxies (GO-6354).

Fig. 2.— HST images of M31 globular clusters. In row order, from top left: 006–058, 064–125, 077–138, 146–000, 156–211, 311–033, 331–057, 468–000, 000–001. All images are in filter F555W or F606W except those of 064–125 and 146–000 (in F300W). All images are 5″ square; 077–138 is not centered in its image because it fell near the edge of a WFPC2 chip.

Fig. 3.— New globular cluster candidates found in HST images. All images are 5″ square.

Fig. 4.— Marginal objects found in HST images: these objects are non-stellar but not obviously star clusters. All images are 5″ square.

Fig. 5.— Possible M31 open clusters found in HST images. All images are 5″ square.

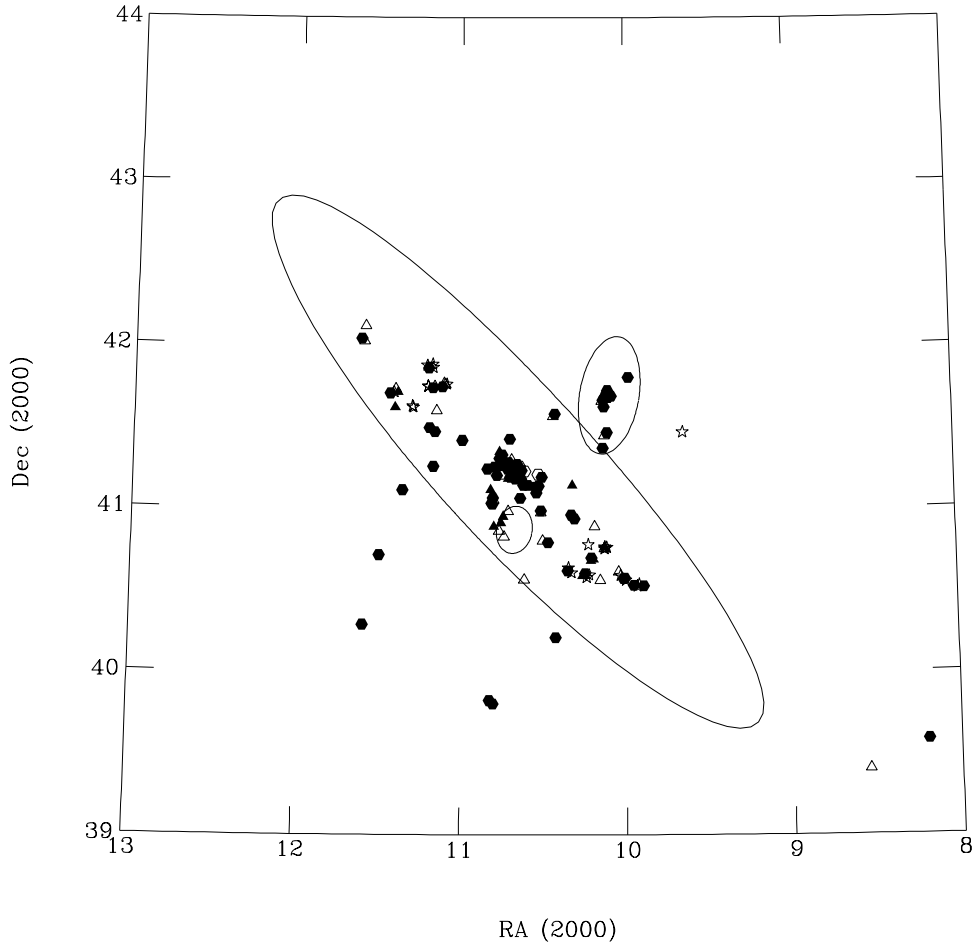

Fig. 6.— Position on the sky of all GCs, GC candidates and open clusters. Ellipses are the same as in Figure 1. Filled symbols are good-quality GC candidates; open symbols are marginal candidates. Hexagons are previously-cataloged objects; triangles are newly-discovered objects; stars are possible open clusters.

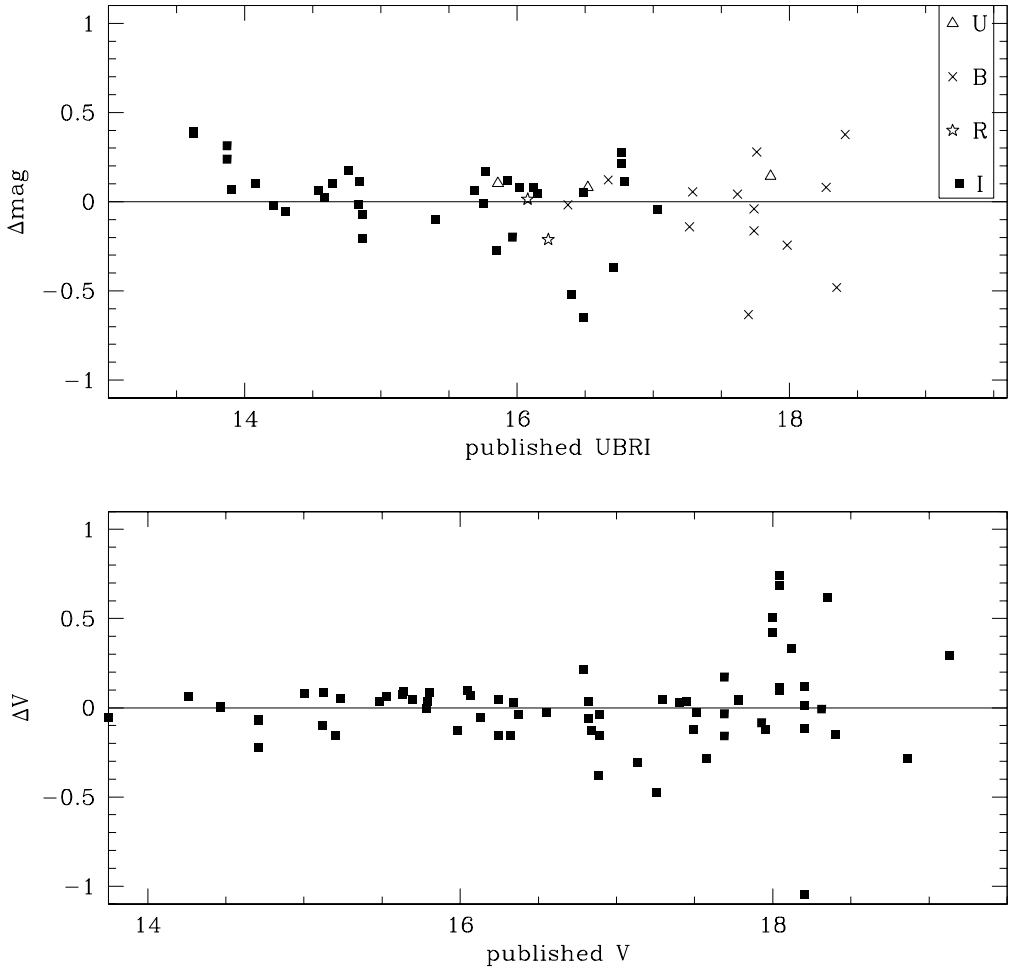

Fig. 7.— Comparison of integrated HST photometry to ground-based photometry: vertical axis is (published photometry)–(HST photometry).

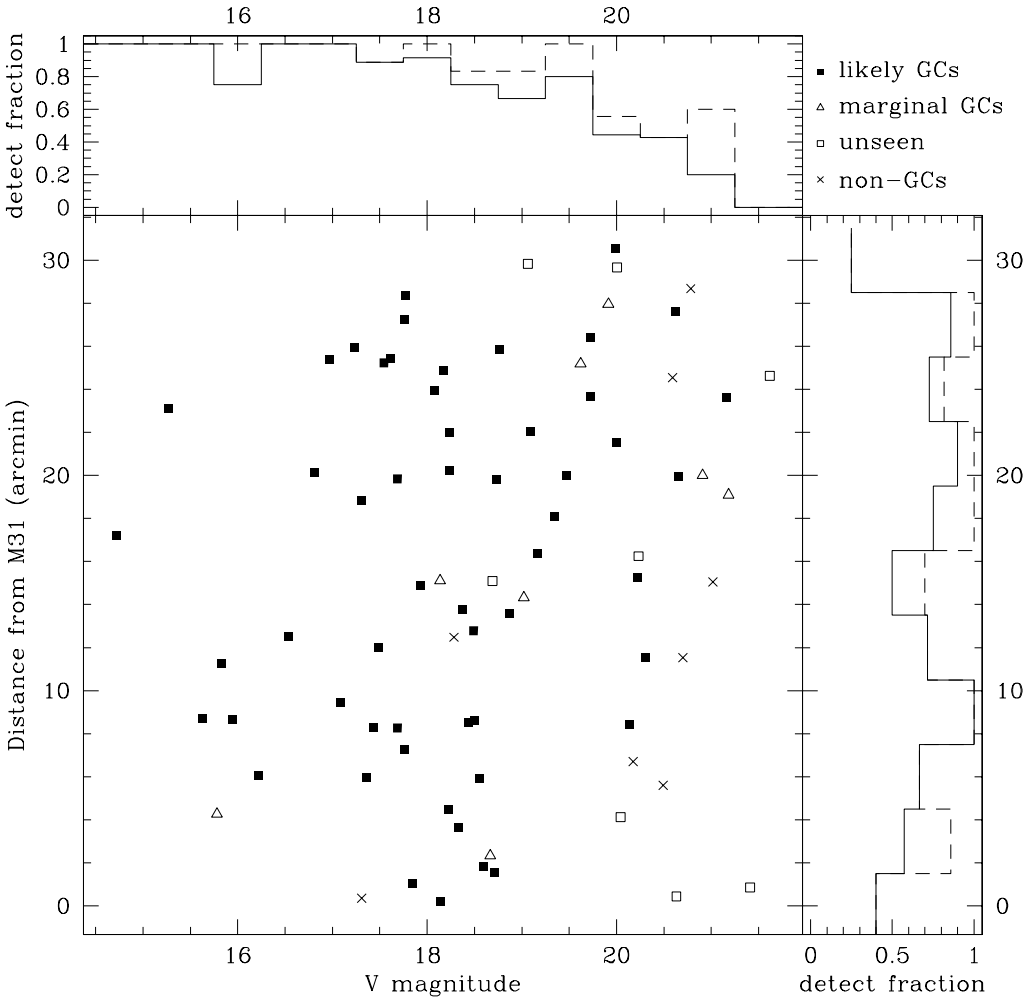

Fig. 8.— Measurement of globular cluster detection efficiency. Large plot: V magnitude vs. R_{gc} for artificial clusters. Symbol type indicates whether an object was detected and how it was classified. The histograms are the fraction of inserted objects detected; solid lines include only A or B class ('good') GCs, and dashed lines include marginal objects.

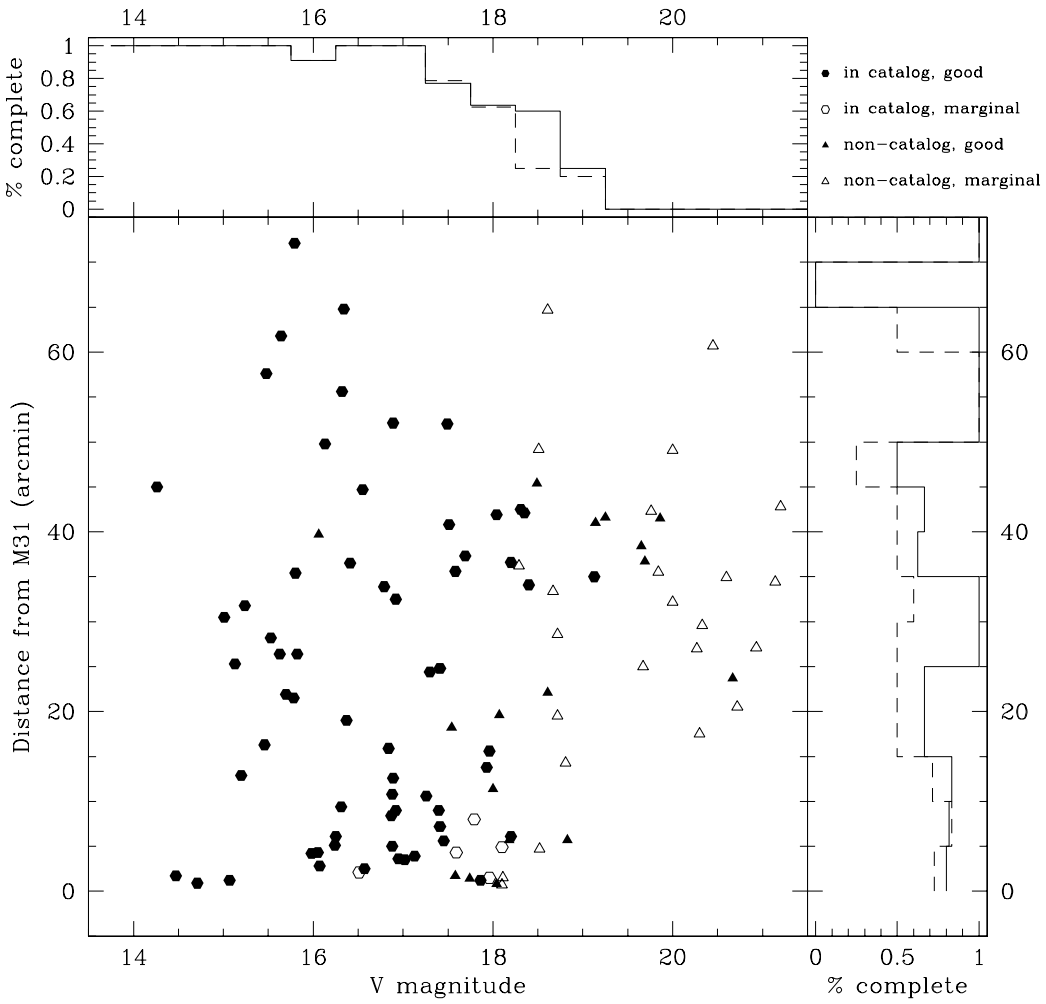

Fig. 9.— Location of previously-cataloged and newly-discovered M31 globular clusters in V vs. R_{gc} space. Symbols indicate object quality and presence in existing catalogs. Histograms estimate the existing catalogs' completeness by showing (number of previously known objects per bin)/(number of known + number of new objects per bin). Solid line histograms include only A or B class GCs, and dashed line histograms include marginal objects.

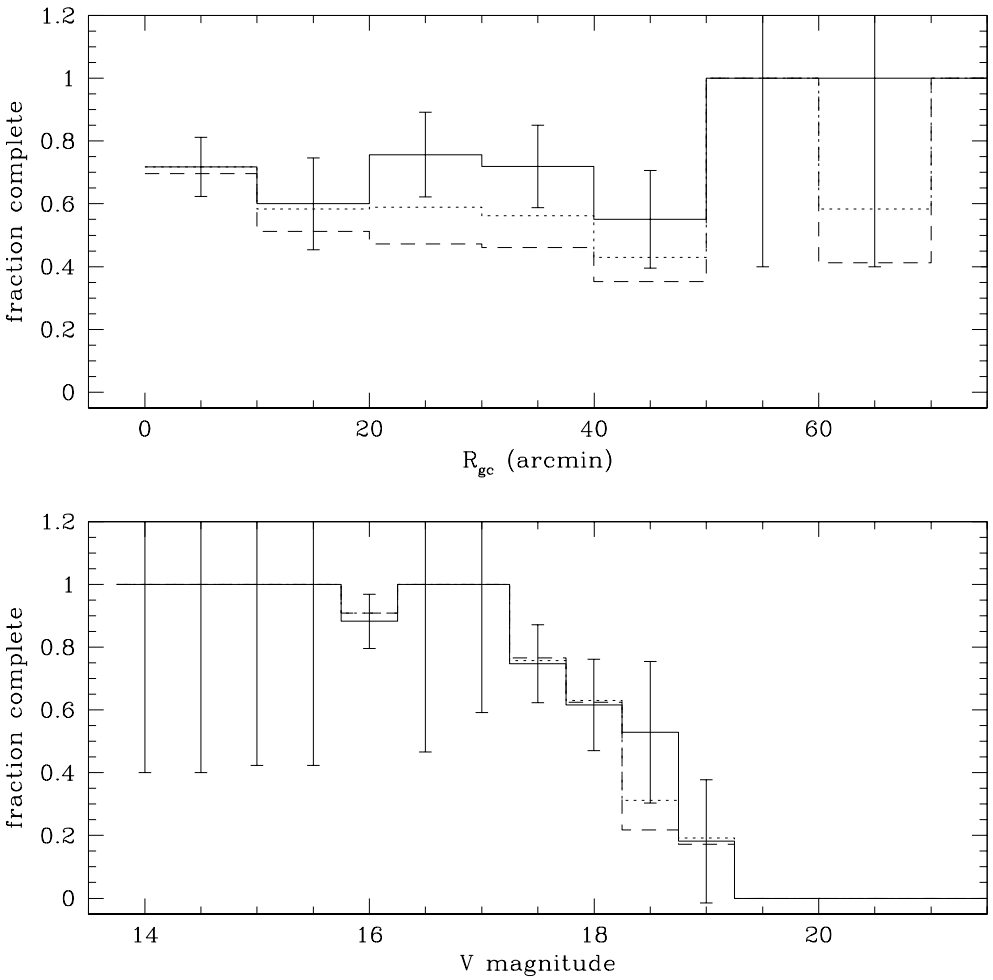

Fig. 10.— Completeness functions for existing surveys of globular clusters in M31. Top panel, $C(R_{gc})$, is summed over entire magnitude range, and bottom panel, $C(V)$, is summed over entire radial range. Different line types reflect different assumptions about how many marginal objects are true M31 clusters. Solid lines: none, dotted lines: half, and dashed lines: all.

Table 1. HST fields used in the search

RA(2000)	Dec (2000)	filter	Exposure[a]	Dataset name
00 32 36.21	+39 27 43.4	F606W	1400	U4K2OI01R
00 32 36.62	+39 27 42.0	F606W	1500	U4K2OI02R
00 32 49.01	+39 35 00.4	F555W	1600	U2E20709T
00 34 13.68	+39 23 26.5	F814W	2800	U2TA0501T
00 34 13.26	+39 23 48.4	F555W	600	U4490401R
00 34 13.46	+39 24 40.5	F702W	600	U27L0501T
00 36 59.20	+39 52 21.3	F555W	800	U4710201M
00 37 43.08	+39 58 00.6	F336W	200	U4F50907R
00 37 49.14	+40 06 29.2	F555W	600	U2782X01T
00 37 58.50	+39 58 32.8	F606W	2100	U67FFP01R
00 38 32.54	+41 28 45.4	F555W	830	U39I0104T
00 38 55.51	+40 20 41.1	F606W	800	U2804I01T
00 39 32.23	+40 30 48.1	F555W	5300	U4CA0701R
00 39 47.35	+40 31 58.0	F555W	1200	U5BJ0101R
00 39 53.99	+41 47 19.2	F555W	2600	U3KL1004R
00 40 01.58	+40 34 14.8	F555W	1200	U5BJ0201R
00 40 10.11	+40 46 08.9	F814W	200	U4WOAH05R
00 40 14.10	+40 37 11.4	F555W	160	U2YE0703T
00 40 14.86	+40 49 02.8	F814W	200	U4WOC605R
00 40 15.76	+40 36 48.1	F300W	1200	U2M80C01T
00 40 22.15	+41 41 38.4	F336W	400	U2GH020CT
00 40 23.16	+41 40 55.6	F555W	2600	U3KL0704M
00 40 23.66	+41 41 55.2	F555W	2600	U3KL0804R
00 40 23.77	+41 41 40.8	F555W	100	U2EE0506T
00 40 25.50	+41 42 25.7	F555W	2600	U3KL0904R
00 40 26.84	+41 27 27.3	F555W	2000	U2830103T
00 40 29.18	+41 36 31.9	F814W	5400	U3KL0501M
00 40 29.40	+40 43 58.3	F814W	400	U2AB0103T
00 40 30.61	+40 44 50.5	F336W	400	U4F51107R
00 40 31.26	+40 42 59.6	F336W	400	U4F51007R
00 40 33.17	+40 45 39.0	F606W	350	U2G20701T
00 40 33.81	+41 39 40.2	F555W	2600	U3KL0604M
00 40 34.22	+41 22 06.5	F555W	5300	U4CA0201R

Table 1—Continued

RA(2000)	Dec (2000)	filter	Exposure[a]	Dataset name
00 40 39.54	+40 33 25.5	F555W	520	U34L6903R
00 40 39.75	+40 53 24.0	F555W	300	U2G20E03T
00 40 46.06	+39 35 01.0	F814W	130	U4WOAU05R
00 40 50.80	+40 41 16.7	F555W	400	U2Q00101T
00 40 56.68	+40 35 29.0	F555W	5300	U4CA0101R
00 40 59.08	+40 46 42.1	F606W	1050	U581OL01R
00 40 59.54	+41 03 38.4	F439W	800	U2TR0804T
00 41 16.28	+40 56 12.6	F555W	5300	U4CA0301R
00 41 17.85	+41 09 00.7	F814W	3700	U2OT0O01T
00 41 22.08	+40 37 06.7	F555W	1200	U5BJ0301R
00 41 38.85	+39 35 39.8	F814W	130	U4WOBK05R
00 41 42.21	+40 12 22.4	F814W	2000	U2830201T
00 41 43.30	+41 34 20.4	F555W	2000	U2830303T
00 41 53.85	+40 50 30.2	F814W	1200	U2806A02T
00 41 55.58	+40 47 15.0	F555W	5300	U4CA0601R
00 42 05.02	+41 12 14.9	F300W	2300	U2OU7501T
00 42 05.27	+40 57 33.9	F555W	520	U34L7003R
00 42 06.07	+41 07 55.5	F814W	6200	U3B83Y01T
00 42 14.14	+41 10 22.6	F606W	160	U2OURQ01T
00 42 14.36	+41 06 24.7	F606W	1800	U581R201R
00 42 14.40	+41 10 11.7	F555W	8400	U3D90207T
00 42 18.01	+40 45 03.7	F555W	900	U3DG0107T
00 42 27.21	+41 08 28.0	F300W	1600	U2OUUT01T
00 42 28.88	+41 03 05.2	F606W	800	U4K2RG01R
00 42 31.00	+41 10 12.2	F814W	400	U4WO9N05R
00 42 32.47	+41 13 39.5	F555W	5200	U2Y30204T
00 42 32.70	+40 33 55.5	F555W	1200	U3YK0101R
00 42 35.13	+41 10 35.1	F555W	5200	U2Y30305T
00 42 38.97	+41 15 29.2	F555W	1680	U2KJ0109T
00 42 39.28	+40 51 42.2	F814W	600	U2E20401T
00 42 39.49	+40 51 46.9	F555W	104	U2LG0101T
00 42 39.88	+41 10 48.9	F814W	400	U42Z2302R
00 42 40.85	+41 15 51.2	F555W	2500	U5LT0104R

Table 1—Continued

RA(2000)	Dec (2000)	filter	Exposure[a]	Dataset name
00 42 40.96	+40 51 07.3	F555W	110	U2EE0405T
00 42 41.68	+40 51 04.3	F555W	2000	U2880704T
00 42 41.74	+41 15 57.9	F814W	600	U2E20201T
00 42 42.21	+40 52 22.4	F555W	1200	U2E20307T
00 42 44.64	+41 16 39.2	F555W	1680	U2E2010BT
00 42 46.91	+41 16 15.9	F555W	2200	U2LG0201T
00 42 47.63	+41 16 11.0	F336W	460	U2LH0103T
00 42 50.04	+41 36 17.8	F814W	700	U4WOC805R
00 42 50.15	+40 59 56.0	F814W	8000	U2OQ3201T
00 42 50.34	+41 17 54.4	F814W	7000	U2OQF801T
00 42 51.45	+41 06 52.9	F814W	400	U4WOA305R
00 42 52.07	+41 24 53.4	F814W	6700	U2OQF301T
00 42 52.26	+41 08 06.8	F814W	4500	U26KCZ01T
00 42 52.37	+41 10 31.7	F814W	400	U42Z3402R
00 42 52.73	+40 56 30.4	F814W	2000	U4XI0101R
00 42 53.03	+41 14 23.4	F814W	400	U42Z1102R
00 42 54.11	+41 08 08.9	F814W	800	U4WOA205R
00 42 54.87	+41 10 35.0	F814W	700	U4WOBC05R
00 42 58.84	+40 50 34.3	F814W	4400	U3VJ0103R
00 43 00.93	+41 13 17.7	F300W	2600	U31K0109T
00 43 01.94	+41 19 19.9	F555W	5200	U38K0103T
00 43 04.61	+40 54 33.0	F555W	2000	U2880801T
00 43 05.28	+40 50 37.8	F300W	5400	U27H0F01T
00 43 05.38	+40 56 40.4	F606W	350	U4G40104R
00 43 06.12	+41 12 59.7	F555W	2000	U5850103R
00 43 06.14	+41 13 00.0	F555W	2000	U5850107R
00 43 06.19	+40 56 52.0	F606W	350	U4G40103R
00 43 06.40	+40 56 31.2	F814W	350	U4G40101R
00 43 07.21	+40 56 42.8	F814W	260	U4G40102R
00 43 07.85	+40 53 32.8	F814W	1100	U4C80403R
00 43 08.59	+41 14 51.7	F300W	8400	U27H0E01T
00 43 09.06	+40 51 18.6	F814W	1000	U4WOBJ05R
00 43 12.49	+41 02 02.7	F606W	350	U4G40204R

Table 1—Continued

RA(2000)	Dec (2000)	filter	Exposure[a]	Dataset name
00 43 12.82	+41 02 17.0	F606W	350	U4G40203R
00 43 13.76	+41 01 59.0	F814W	350	U4G40201R
00 43 14.09	+41 02 13.3	F814W	260	U4G40202R
00 43 18.05	+39 49 13.1	F814W	2000	U2830401T
00 43 20.30	+41 05 36.2	F814W	400	U42Z1202R
00 43 20.80	+41 06 14.5	F814W	300	U42Z4602R
00 43 22.39	+41 13 53.8	F814W	1500	U2OT0S01T
00 43 25.28	+41 04 02.2	F814W	4400	U3VJ0203R
00 43 36.72	+41 26 15.4	F555W	350	U2KW0601T
00 43 43.26	+41 00 32.4	F814W	400	U4WOA105R
00 43 46.58	+41 11 14.7	F814W	300	U42Z5702R
00 43 47.85	+41 11 00.6	F814W	300	U42Z5802R
00 43 54.55	+41 24 10.8	F300W	600	U2M80G01T
00 43 57.06	+41 25 33.4	F300W	600	U2M80H01T
00 44 14.38	+41 20 45.2	F336W	400	U4F51207R
00 44 23.45	+41 20 40.8	F336W	320	U4F51307R
00 44 23.74	+41 45 16.3	F555W	800	U4710101M
00 44 34.81	+41 38 38.4	F336W	800	U5750101R
00 44 35.25	+41 31 21.6	F814W	500	U4WOBH08R
00 44 36.29	+41 35 05.6	F814W	500	U4WOBS05R
00 44 42.45	+41 44 24.2	F555W	5300	U4CA0401M
00 44 42.52	+41 44 24.1	F555W	5300	U4CA0501R
00 44 42.59	+41 14 30.3	F814W	500	U4WOA005R
00 44 44.23	+41 27 33.9	F555W	140	U2Y20106T
00 44 46.19	+41 51 33.4	F555W	1200	U5BJ0401R
00 44 49.34	+41 28 59.0	F555W	140	U2Y20206T
00 44 50.61	+41 19 11.1	F555W	3800	U2GV0401T
00 44 51.22	+41 30 03.7	F555W	160	U2YE0603T
00 44 57.63	+41 30 51.7	F555W	140	U2Y20306T
00 45 00.36	+41 31 55.1	F300W	600	U2M80A01T
00 45 03.79	+41 31 09.6	F300W	600	U2M80E01T
00 45 05.66	+41 38 00.4	F336W	320	U4F51407R
00 45 07.76	+41 36 46.8	F336W	280	U4F51507R

Table 1—Continued

RA(2000)	Dec (2000)	filter	Exposure[a]	Dataset name
00 45 09.25	+41 34 30.7	F555W	140	U2Y20406T
00 45 11.95	+41 36 57.0	F555W	140	U2Y20506T
00 45 28.46	+41 05 53.9	F555W	4320	U2UG010AT
00 45 36.98	+41 42 17.3	F606W	2300	U5HNM301R
00 45 38.15	+41 36 02.4	F300W	650	U4WOBG0ER
00 45 39.00	+41 36 36.3	F814W	580	U4WOBG09R
00 45 39.25	+41 36 32.4	F606W	1140	U4WOBG01R
00 46 01.64	+40 41 58.3	F555W	4320	U2UG020AT
00 46 20.46	+40 16 34.1	F555W	5300	U4CA0801R
00 46 24.33	+42 07 01.7	F814W	350	U4WOC905R
00 46 24.56	+42 01 38.7	F555W	5300	U4CA0901R
00 46 29.85	+42 04 50.4	F336W	320	U4F51707R
00 48 15.15	+40 26 31.0	F606W	1000	U36Z7801R
00 48 21.29	+40 29 02.4	F606W	1000	U36Z8401R
00 48 42.83	+40 24 47.2	F606W	1000	U36Z7701R
00 48 44.22	+40 33 06.0	F606W	1000	U36Z8201R
00 49 08.22	+40 30 33.9	F606W	1000	U36Z8301R
00 49 13.48	+40 21 51.1	F606W	1000	U36Z8001R
00 49 18.35	+40 30 12.0	F606W	1000	U36Z8501R
00 49 28.48	+40 21 54.4	F606W	1000	U36Z8101R
00 49 31.26	+40 27 57.9	F606W	1000	U36Z8601R
00 50 06.13	+41 33 56.0	F606W	2100	U67FGY01R

[a]'Exposure' is the combined exposure time, in seconds, of all images in the specified filter and position.

Table 2. Cataloged objects which are not M31 globular clusters

name	class[a]	HST field(s)
000-253	star	U2M80H01T[4]
000-M046	HII region?	U2Y20106T[2]
000-M050	HII region?	U4WOBH08A[4]
000-M068	stars	U4F51407A[4]
000-V211	stars	U2TR0804B[4]
000-V212	star	U2TR0804B[1]
000-V298	star	U2Y20206T[4]
064D-NB80	star	U2KJ0109A[3]
074D-NB88	star	U2LH0103B[4] U2LG0201B[4] U42Z1102R[3]
075D-NB96	star	U2LH0103B[4] U2LG0201B[4]
080D-NB93	star	U2LH0103B[3] U2LG0201B[3]
084D-000	star	U2OQF801A[3]
086D-000	star	U3VJ0103A[3]
093D-000	star	U27H0F01B[3]
114D-000	star	U4710101A[4]
133-191	stars	U2OQF301A[4]
138-000	star	U2OQF801A[3]
166-000	star	U2OT0S01A[4]
185D-000	star	U5BJ0201A[3]
193D-055	star	U2EE0506T[3] U3KL0804A[4] U3KL0904A[1]
254D-000	star	U5BJ0401A[4]
285-000	galaxy	U2UG010AA[2]
326-000	star	U2EE0506T[1] U3KL0804A[2] U2GH020CA[1]
332-000	star	U3KL0704A[4]
444-000	star	U2EE0506T[2] U3KL0704A[2] U3KL0804A[3]
446-000	galaxy	U3KL0501A[4]
501-345	galaxy	U36Z8401A[1]
NB100	star	U31K0109B[3]
NB103	star	U42Z1102R[4]
NB104	star	U42Z1102R[1]
NB106	star	U31K0109B[4]
NB26	star	U31K0109B[3]
NB27	star (pr)	U2Y30204A[2]

Table 2—Continued

name	class[a]	HST field(s)
NB30	star (pr)	U2E2010BA[3]
NB37	star	U2KJ0109A[4]
NB42	star (pr)	U2E2010BA[3] U2LH0103B[2] U2OQF801A[1]
NB44	star	U2E2010BA[3]
NB45	star	U42Z1102R[3]
NB49	star	U42Z1102R[2] U31K0109B[3]
NB51	stars (pr)	U2Y30204A[3]
NB53	star	U2KJ0109A[3]
NB54	star	U2Y30204A[3]
NB56	star	U2Y30204A[4]
NB75	star	U2KJ0109A[4]
NB76	star	U2KJ0109A[4]
NB78	star	U2KJ0109A[3] U5LT0104A[3]
NB82	stars (pr)	U2Y30204A[3]
NB84	star (pr)	U2Y30204A[3]
NB85	star (pr)	U2Y30204A[3]
NB94	star	U2LH0103B[4] U2LG0201B[4]
NB95	star	U2LH0103B[4] U2LG0201B[4]
NB97	star	U42Z1102R[1]
NB99	star	U31K0109B[3] U42Z1102R[2]
000-D040	blank	U4CA0101A[4]
000-M023	blank	U4F51307B[4]
000-M056	blank	U4F51407A[3]
000-M060	blank	U4F51407A[4]
038D-000	blank	U2OU7501T[3]
092D-000	blank	U31K0109B[2]
353-000	blank	U2LH0103B[4] U2LG0201B[4] U5LT0104A[2]
NB18	blank	U2OQF801A[2]
NB38	blank	U2Y30204A[2]
NB40	blank	U42Z1102R[2]
NB57	blank	U2Y30204A[2]
NB58	blank	U5LT0104A[2] U2E20201A[2] U2KJ0109A[2]
NB59	blank	U2LH0103B[4] U42Z1102R[4]

Table 2—Continued

name	class[a]	HST field(s)
NB74	blank	U2E2010BA[2] U2E20201A[4] U5LT0104A[4]
NB87	blank	U2OQF801A[2]

[a]'pr' refers to objects which have slightly larger FWHMs than most stars, although we still believe them to be stars. 'stars' refers to objects which appear to be blended images of 2 or 3 stars. 'Blank' refers to a object which was not detected at its catalog coordinates.

Table 3. New globular cluster candidates found in M31 HST fields

name	RA(2000)	Dec (2000)	quality	comments
M31GC J003411+392359	00 34 11.48	39 23 59.1	C/D	···
M31GC J004010+403625	00 40 10.33	40 36 24.7	C/D	···
M31GC J004023+414045	00 40 22.68	41 40 44.5	C	···
M31GC J004027+414225	00 40 27.25	41 42 24.8	B	···
M31GC J004030+404530	00 40 30.46	40 45 29.6	B	···
M31GC J004031+404454	00 40 30.63	40 44 54.3	C	···
M31GC J004031+412627	00 40 30.68	41 26 27.1	C	···
M31GC J004034+413905	00 40 34.42	41 39 04.8	C/D	···
M31GC J004037+403321	00 40 37.15	40 33 21.4	C	···
M31GC J004045+405308	00 40 44.92	40 53 07.6	C	···
M31GC J004051+404039	00 40 50.68	40 40 38.6	B/C	···
M31GC J004103+403458	00 41 02.88	40 34 57.9	B	Hodge 119?
M31GC J004146+413326	00 41 45.57	41 33 26.2	C	···
M31GC J004200+404746	00 42 00.39	40 47 45.8	C	···
M31GC J004228+403330	00 42 27.56	40 33 29.8	C/D	···
M31GC J004246+411737	00 42 46.01	41 17 36.5	C	···
M31GC J004251+405841	00 42 50.80	40 58 40.7	C	···
M31GC J004251+411035	00 42 50.78	41 10 34.7	A	···
M31GC J004257+404916	00 42 57.05	40 49 16.4	C	Hodge 195?
M31GC J004258+405645	00 42 58.02	40 56 45.4	A	···
M31GC J004301+405418	00 43 01.35	40 54 17.5	B	···
M31GC J004304+405129	00 43 04.27	40 51 29.2	C	···
M31GC J004304+412028	00 43 03.75	41 20 28.2	A	···
M31GC J004312+405303	00 43 11.86	40 53 02.8	B	···
M31GC J004312+410249	00 43 11.99	41 02 49.1	C	···
M31GC J004424+414502	00 44 23.71	41 45 02.3	C	X-ray src: SHP278?
M31GC J004425+414529	00 44 25.21	41 45 29.1	C/D	···
M31GC J004439+414426	00 44 39.07	41 44 26.3	C	···
M31GC J004537+413644	00 45 37.25	41 36 44.3	B	···
M31GC J004537+414332	00 45 36.75	41 43 32.2	C	···
M31GC J004622+420631	00 46 21.80	42 06 30.8	C	···
M31GC J004624+420059	00 46 23.50	42 00 58.5	C	···
M31OC J003836+412739	00 38 35.73	41 27 39.3	B	···

Table 3—Continued

name	RA(2000)	Dec (2000)	quality	comments
M31OC J003941+403154	00 39 40.52	40 31 53.6	C	···
M31OC J003943+403116	00 39 43.21	40 31 15.6	C	···
M31OC J004000+403326	00 39 59.99	40 33 25.9	C	···
M31OC J004008+403507	00 40 07.55	40 35 06.6	B	···
M31OC J004027+404524	00 40 27.26	40 45 23.7	C	···
M31OC J004031+404537	00 40 30.51	40 45 37.4	C	···
M31OC J004053+403519	00 40 52.94	40 35 19.2	D	···
M31OC J004054+404625	00 40 54.14	40 46 24.7	C	···
M31OC J004057+403425	00 40 56.62	40 34 24.7	C	···
M31OC J004119+403608	00 41 18.69	40 36 08.2	B/C	···
M31OC J004123+403756	00 41 23.30	40 37 56.1	C	···
M31OC J004421+414516	00 44 21.44	41 45 15.9	C	···
M31OC J004442+415122	00 44 41.84	41 51 22.4	C	···
M31OC J004442+415237	00 44 42.25	41 52 36.7	C	···
M31OC J004449+414430	00 44 48.83	41 44 30.3	C/D	···
M31OC J004450+415211	00 44 50.27	41 52 11.1	C	···
M31OC J004510+413646	00 45 10.45	41 36 46.3	C	Hodge 311?
M31OC J004512+413712	00 45 11.81	41 37 11.6	C	H II region, Hodge 313?
M31OC J004539+414220	00 45 38.88	41 42 20.4	C	Radio src MY0042+414?

Table 4. Photometry of new clusters and candidates in M31 HST fields

name	U^a	B	V	R	I	$\langle r_{1/2} \rangle$ ($''$)
Cataloged clusters						
000–001	···	···	13.807	···	12.684	0.40
000–D38	···	···	19.247	···	18.276	0.37
000–M045	···	19.391	18.723	···	17.446	1.49
000–M91	···	···	19.143	···	···	0.89
006–058	···	···	15.463	···	14.354	0.38
009–061	···	···	···	···	15.809	0.71
011–063	···	···	16.578	···	15.624	0.31
012–064	···	···	15.042	···	13.979	0.42
018–071	···	···	17.533	···	16.385	1.14
020D–089	···	···	···	···	16.039	0.80
027–087	···	···	15.559	···	14.409	0.41
030–091	···	···	17.377	···	15.593	0.59
045–108	···	···	15.784	···	14.477	0.42
058–119	···	···	14.925	···	13.837	0.36
064–125	17.461*	···	···	···	···	0.69
068–130	···	17.575	16.407	···	14.849	0.68
070–133	···	···	17.262	···	16.165	0.20
071–000	22.716*	···	···	···	···	0.07
076–138	17.720	17.483	16.927	···	15.626	0.53
077–139	···	18.829	17.734	···	16.125	0.42
092–152	18.766*	···	···	···	···	0.41
097D–000	···	···	···	17.878	17.121	1.08
101–164	18.523*	···	···	···	···	0.42
109–170	···	17.407	16.197	···	14.936	0.61
110–172	···	···	15.355	···	···	0.66
114–175	···	···	17.439	···	15.940	0.47
115–177	···	···	15.997	···	14.560	0.25
118–NB6	···	···	16.431	···	15.207	0.52
123–182	···	···	17.416	16.754	16.126	0.58
124–NB10	16.094	···	14.777	···	13.631	0.53
127–185	15.756	···	14.467	···	13.239	0.75
128–187	···	···	···	16.441	15.764	0.41

Table 4—Continued

name	U^a	B	V	R	I	$\langle r_{1/2} \rangle$ ($''$)
132–000	···	···	17.739	17.244	16.440	0.34
134–190	···	···	···	16.064	15.502	0.52
143–198	···	···	15.954	···	14.731	0.25
145–000	19.901*	···	···	···	···	0.47
146–000	18.458*	···	···	···	···	0.59
148–200	···	···	16.110	···	···	0.51
153–000	18.220*	···	···	···	···	0.38
155–210	···	···	18.011	···	16.672	0.40
156–211	···	···	16.969	···	15.873	0.64
160–214	···	···	18.076	···	17.075	0.52
167–000	···	···	···	···	16.109	0.33
205–256	16.938*	···	···	···	···	0.32
231–285	···	18.227	17.248	···	···	0.48
232–286	16.440	16.391	15.646	···	14.543	0.66
233–287	···	···	15.718	···	14.585	0.41
234–290	···	17.780	16.783	···	···	0.51
240–302	···	···	15.181	···	14.230	0.80
257–000	···	11.907	20.960	···	16.312	0.65
264–000	18.652*	···	17.577	···	16.811	0.67
268–000	···	···	18.314	···	16.880	0.39
279–D068	···	···	18.549	···	16.964	0.68
311–033	···	···	15.445	···	14.215	0.38
315–038	···	16.548	16.473	···	···	0.56
317–041	···	···	16.573	···	15.713	0.73
318–042	···	17.234	17.047	···	···	0.63
319–044	···	18.333	17.608	···	···	0.41
324–051	···	···	18.446	···	17.633	0.30
328–054	···	···	17.861	···	16.918	0.85
330–056	···	···	17.724	···	16.555	0.56
331–057	···	···	18.191	···	17.076	0.56
333–000	···	···	18.840	···	17.711	0.90
338–076	···	···	14.195	···	13.174	0.56
342–094	···	18.033	17.733	···	···	0.92

Table 4—Continued

name	U^a	B	V	R	I	$\langle r_{1/2} \rangle$ ($''$)
343–105	···	···	16.310	···	15.274	0.36
358–219	···	···	15.219	···	14.122	0.55
368–293	···	18.189	17.924	···	···	0.54
374–306	19.128*	···	18.319	···	···	0.68
379–312	···	···	16.183	···	14.936	0.65
384–319	···	···	15.752	···	14.564	0.36
386–322	···	···	15.547	···	14.393	0.36
468–000	···	···	17.788	···	16.626	1.95
NB21	···	···	17.865	···	16.771	0.41
NB39	18.551	···	17.941	···	17.876	0.38
NB41	···	···	18.097	···	17.183	0.43
NB81	···	···	17.025	···	···	0.35
NB83	···	···	17.585	···	16.599	0.25
NB86	···	···	18.522	···	17.446	0.17
NB89	···	···	17.965	···	16.888	0.34
New clusters						
M31GC J003411+392359	···	···	···	22.302	···	4.44
M31GC J004010+403625	···	18.906	18.505	···	···	0.24
M31GC J004023+414045	···	···	18.289	···	16.990	1.08
M31GC J004027+414225	···	···	19.691	···	19.138	0.76
M31GC J004030+404530	···	···	16.064	···	···	0.37
M31GC J004031+404454	···	15.090	22.708	···	20.337	0.29
M31GC J004031+412627	···	···	20.930	···	19.477	0.57
M31GC J004034+413905	···	···	18.666	···	···	7.52
M31GC J004037+403321	···	···	19.773	···	18.773	0.49
M31GC J004051+404039	···	···	19.862	···	18.616	0.73
M31GC J004103+403458	···	···	18.487	···	17.920	0.38
M31GC J004146+413326	···	···	20.716	···	18.826	0.39
M31GC J004200+404746	···	···	20.327	···	19.636	0.45
M31GC J004228+403330	···	···	21.195	···	19.477	0.51
M31GC J004246+411737	19.507*	···	18.111	···	17.706	0.43
M31GC J004251+405841	···	···	20.296	···	19.309	0.20
M31GC J004251+411035	···	19.177	18.178	···	16.886	0.21

Table 4—Continued

name	U[a]	B	V	R	I	$\langle r_{1/2} \rangle$ ($''$)
M31GC J004257+404916	···	···	20.271	···	18.648	1.18
M31GC J004258+405645	···	···	18.066	···	···	0.31
M31GC J004301+405418	···	···	18.613	···	17.290	0.45
M31GC J004304+405129	···	···	19.666	···	18.392	1.12
M31GC J004304+412028	···	···	18.828	···	16.857	0.38
M31GC J004312+405303	···	···	20.670	···	19.150	0.73
M31GC J004312+410249	···	···	18.810	···	18.816	0.52
M31GC J004424+414502	···	···	21.143	···	19.232	0.31
M31GC J004425+414529	···	···	20.597	···	20.580	0.99
M31GC J004439+414426	···	···	19.840	···	18.746	0.67
M31GC J004537+413644	···	20.350	19.648	···	18.724	0.92
M31GC J004537+414332	22.529*	···	19.759	···	···	0.47
M31GC J004622+420631	···	20.085	18.614	···	17.135	2.86
M31GC J004624+420059	···	···	20.445	···	19.188	0.70
M31OC J004539+414220	20.812*	···	20.163	···	···	0.61
M31OC J004027+404524	···	···	18.148	···	18.046	0.55
M31OC J004512+413712	···	18.352	17.466	···	···	0.65
M31OC J003941+403154	···	20.398	20.002	···	···	0.68
M31OC J004123+403756	···	21.752	19.965	···	···	0.78
M31OC J004442+415122	···	19.788	19.533	···	···	1.08
M31OC J004442+415237	···	19.997	19.812	···	···	0.50
M31OC J004450+415211	···	20.599	20.439	···	···	0.40
M31OC J004449+414430	···	···	20.229	···	19.455	0.75
M31OC J004054+404625	···	23.432	22.082	···	21.504	0.18
M31OC J003943+403116	···	20.854	21.014	···	···	0.45
M31OC J004000+403326	···	19.232	19.006	···	···	1.09
M31OC J004031+404537	···	···	17.806	···	···	4.75
M31OC J004057+403425	···	···	18.756	···	18.675	0.86
M31OC J004053+403519	···	···	18.579	···	18.634	0.99
M31OC J003836+412739	···	···	20.406	···	···	1.43
M31OC J004008+403507	···	20.773	20.298	···	···	0.84
M31OC J004119+403608	···	···	19.501	···	···	1.88

[a]Asterisks indicate F300W, instead of standard U-band magnitudes.